Statistical Properties of SGR J1550-5418 Bursts

Nicholas M. Gorgone[†]

Connecticut College, 270 Mohegan Ave., New London, CT, 06320

Abstract

Magnetars are slowly rotating neutron stars with extreme magnetic fields, over 10^{15} Gauss. Only few have been discovered in the last 30 years. These sources are dormant most of their lifetimes and become randomly active emitting multiple soft gamma-ray bursts. We present here our results on the temporal analysis of ~300 bursts from Soft Gamma Repeater SGR J1550-5418 recorded with the Gamma-ray Burst Monitor (GBM) onboard the Fermi Observatory during its activation on January 22-29, 2009. We employed an un-triggered burst search in the energy range 8-100keV to collect all events from the source, besides the ones that triggered GBM. For the entire sample of bursts we determined their durations, rise and decay times. We study here the statistical properties of these characteristics and discuss how these may help us better understand the physical characteristics of the magnetar model.

I. Introduction

GBM uses an array of 12 sodium iodide (NaI(Tl)) and two bismuth germinate (BGO) scintillation detectors to detect gamma rays from ~8keV to ~1MeV and ~200keV to ~40 MeV, respectively, giving GBM with an energy range sensitive from ~8keV to ~40 MeV.[1] The configuration of the detectors on the spacecraft gives GBM a view of approximately 70% of the sky at any given time. Since it's launch roughly two years ago, GBM has successfully identified 524 Gamma Ray Bursts (GRBs) and other transient cosmic phenomena such as solar flares, cosmic ray showers and terrestrial gamma-ray flashes (TGFs). Soft gamma ray bursts from a magnetar is the focus of our paper.

A magnetar or soft gamma repeater (SGR) is a neutron star that is currently thought to possess an extreme magnetic field $> 10^{14}$ G. It randomly emits hard X-ray - soft gamma-ray bursts that last from tens to hundreds or milliseconds. The GBM is perfect for measuring bursts emitted by SGRs because the spectral peak of these bursts has been found to lie within the ~8 keV to ~100keV range.[1]

SGRs are very rare; less than 20 have been discovered thus far. A SGR is formed when a massive star reaches the end of its life and undergoes a supernova explosion. Once the core collapses and the outer layers of the star are ejected, all that is left is a spinning ball of neutrons at nuclear densities. If certain conditions apply (high convection and spin rates) the final outcome of these explosions is a magnetar. These stars have the strongest magnetic fields measured in the universe.

II. SGR J1550-5418

When SGR J1550-5418 was first observed as a magnetar it was classified as an anomalous x-ray pulsar (AXP 1E1547.0-5408), another class of neutron star believed to have extreme B-fields. The

---

1 Charles Meegan et. al. 2009, ApJ

source is located in our galaxy and has a known spin period of 2.07 s. The first SGR-like outburst in X-rays observed from this source was in October of 2008. Although there were few bursts and they were relatively weak, this activation identified AXP 1E1547.0-5408 as a new SGR candidate. Observers began monitoring it more closely to determine if it would continue bursting within the right energy range to classify it as a true SGR.

On January 22, 2009 it became extremely active and began exhibiting SGR behavior. Huge numbers of bursts at different intensity levels were recorded during the rest of that day and in the following week. Bright bursts with long durations as well as short, weak bursts continued to be emitted from the star and were recorded in the months that followed.

III. Sample of Bursts

Not all bursts identified in each detector were suitable for analysis. We systematically down-selected from the initial pool of data using the following criteria in order to achieve a good, consistent sample.

A. Un-triggered Burst Search

GBM experiences a down time of approximately 10 minutes after a source triggers the instrument, during which it cannot trigger again. Because of bursts in rapid succession on January 22-29, many bursts from SGR J1550-5418 were cataloged within one trigger time. All data recorded within each of these 10-minute time frames as well as the continuously-recorded CTIME data were examined to find correct trigger times for each event. An event was was defined as a burst if the detector with highest and second highest fluence levels were $> 5.5\sigma$ and $> 4.5\sigma$ above background levels, respectively. The un-triggered burst search effectively assigned a trigger time to each of the 356 bursts in our Jan. 22-29 time frame.

To further delineate bursts within the un-triggered burst search, we defined bursts as single- or multi-peaked events following Göğüş et al. (ApJ 2001). To qualify as two single events, the time (Δt) between the peaks must be greater than a quarter of the spin period of the SGR, and the count rate level must drop to the background noise level between the peaks. For SGR J1550-5418 the period is 2.07 sec, and therefore $\Delta t > 0.5$ sec.

Because some of the multi-peaked events had been assigned multiple trigger times by the un-triggered burst search, we used the technique described to narrow our original 356-burst sample to 295 bursts. We then separated out sample into 93 single-peaked events and 178 multi-peaked events for use in the rise time, T_r, parameter calculations. For rise time we did not use 23 bursts which saturated our detectors (see §§ III.D).

B. Fine Time-binning

We only used data from the un-triggered burst search for which fine time binning is available. Time Tagged Event (TTE) data contain the arrival times and energies of individual gamma-rays at very high time resolution (up to 10 μs). When a signal is strong enough to trigger GBM the onboard data bus stores TTE data for the time interval of 30 s before the instrument triggers to 300 s after it. Because of the short time duration of SGR bursts, a finer time binning than the normal CTIME binning of 64 ms must be used.

C. Viewing Angle and Detector Blockage

To determine which of the NaI(Tl) detectors onboard Fermi to utilize, we calculated which detectors had the smallest viewing angles to the source, ϕ, for every burst (see Fig. 1). Detectors with source angles $\geq 60°$ were disregarded. We then used an IDL program written by Vandiver Chaplin[2] which is based on an area intersection algorithm to figure out which detectors are blocked by the Large Area Telescope (LAT) and radiators onboard

Figure 1. NaI(Tl) detector with viewing angle, ϕ, between the yellow source vector and the

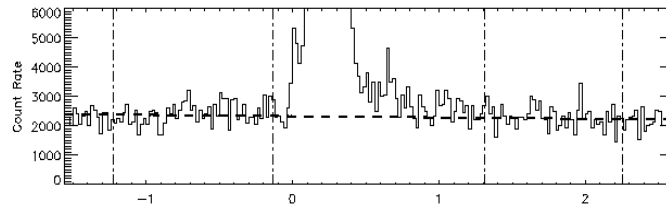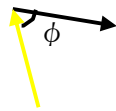Fermi at any given time (see Fig. 2). We chose only unblocked detectors for our analysis.
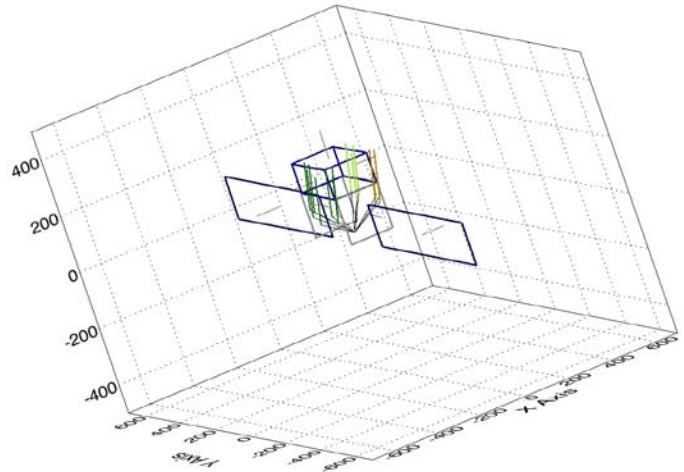
Figure 2. Detectors with light green lines are blocked by the LAT, brown by a radiator and the detectors with dark green lines see

D. Detector Saturation

The NaI(Tl) detectors can only measure a count rate up to a maximum of ~375 kHz. When this rate is exceeded, the instrument continues to take data at this level and truncates all higher count rate values (see
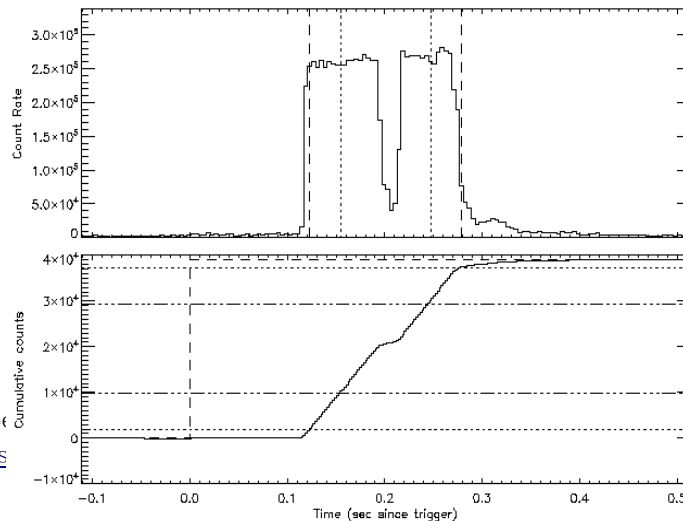
Figure 3. A bright burst which saturated the

figure 3, middle panel). A total of 23 bursts from the un-triggered burst search saturated our instrument. These bursts were used in our statistical analysis of T_{90} ($_{50}$), τ_{90} ($_{50}$), and δ_{90} ($_{50}$) but omitted for our rise time, T_r, analysis (for a definition of these parameters, see §IV).

IV. Analysis and Results

A. Computation Techniques

To calculate the temporal parameters of the un-triggered bursts we used an IDL program written by Ersin Göğüş[3] and modified by Lin Lin[4]. It uses several steps to determine these parameters for each burst. First, we selected which detectors to use. We chose detectors as described in §III. After this, the program adds the count rates of all selected detectors then plots count rate vs. time (Fig. 3, top panel). From this plot the we selected intervals before and after the main burst that contain only background noise. The program fits the selections to first or second order polynomial and subtracts the fit from t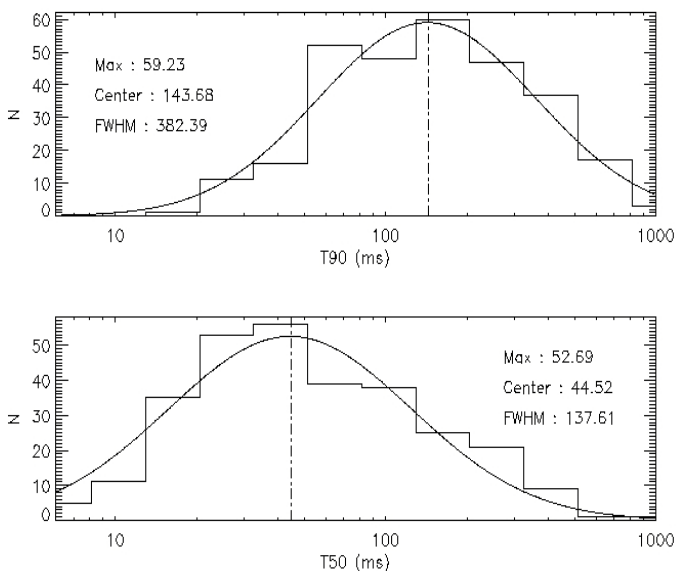he entire light curve. It then plots the background-subtracted light curve as count rate vs. time (Fig. 3, middle panel). We then selected pre- and post-burst intervals, and the program fits the background-subtracted light curve with a combination of a linear model and a step function. Finally, it plots the background-subtracted cumulative light curve vs. time (Fig. 3, bottom panel) and determines the temporal parameters.

Figure 4. *Distributions of T_{90} and T_{50} top and*
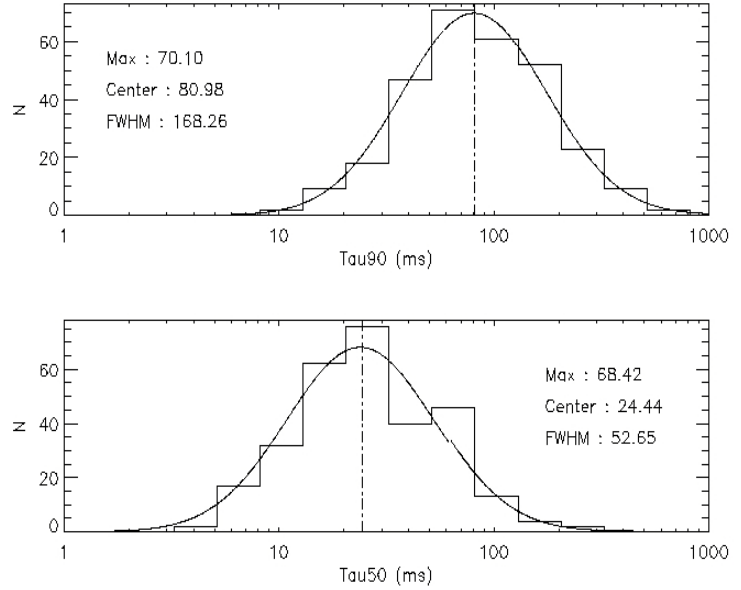
B. T_{90} and T_{50} durations

The T_x duration is the time it takes a burst to accumulate x% of the counts within the selected energy range. The T_{90} is the duration between the 5% and 95% cumulative count levels defined by a piecemeal step function (see Fig. 3). For T_{50} the duration is measured between the 25% and 75% levels. From our sample of 294 individual bursts from the un-triggered burst search we plotted a histogram of frequency vs. time for T_{90} and T_{50} individually and fitted each to a log-normal function (see Fig. 4).

We compared the T_{90} function peak to those calculated by Göğüş et al. (2001) for SGRs 1806-20 and 1900+14 (see §§IV.F, Table 1). For SGR J1550-5418 we found the log-normal peak to be at 143.7 ms. This value is comparable to the 161.8 ms determined for SGR 1800-20, and a factor of two larger than the 92.4 ms peak of SGR 1900+14.

---

3 Sabanci University faculty

4 CSPAR, University of Alabama in Huntsville, Alabama, USA, The National Astronomical
   Observatories, Graduate University of Chinese Academy of Sciences, Beijing 100049, China

C. τ_{90} and τ_{50} durations

The τ_y duration is equal to the sum of all time bins with a count rate $\geq$ y% of the total count rate within the event. Similar to the T durations, we plotted a frequency vs. time histogram and fitted log-normal curves to the distributions of our sample (see Fig. 5). Again comparing results with Göğüş et al. (2001) for τ_{90} , we found the fitted peak, 81.0 ms, to be comparable to the 82.3 ms measured for SGR 1800-20. These duration times are both greater than the 49.6 ms for SGR 1900+14.

Figure 5. Distributions of τ_{90} and τ_{50} top and bottom panels, respectively, plotting frequency

D. Duty cycles δ_{90} and δ_{50}

Duty cycle 90, δ_{90}, is the ratio of τ_{90} over T_{90} and is essentially a measure of efficiency of the burster. The duty cycle 50, δ_{50}, parameter can be calculated similarly. Using the T_{90}s and T_{50}s from §§IV.B and the τ_{90}s and τ_{50}s from §§IV.C, we calculated the duty cycle 90s and 50s for all the bursts in our sample, plotted them as a frequency vs. duty cycle histogram, and fitted the distributions to a normal curve (see Fig.6).
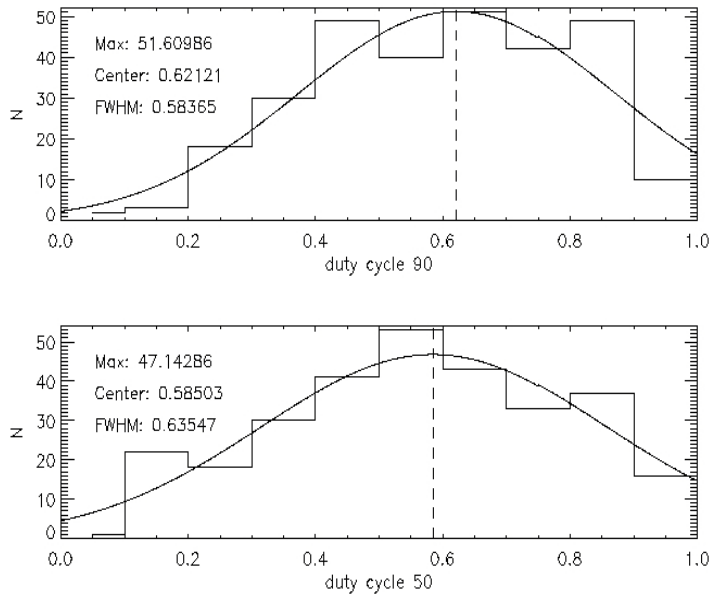
Both SGRs sampled by Göğüş et al. (2001) had a fitted peak at ˜0.45 while the peak for SGR J1550-5418 was 0.65.

E. Rise time, T_r

Rise time is the time it takes a burst to achieve its maximum count rate value. It is calculated by subtracting the onset of T_{90} time from the peak time. When this value is compared to T_{90} via the ratio of T_r/T_{90} we can see what percentage of time during the T_{90} is used reaching the peak of the burst. We separated our burst sample into single-peaked events and multi-peaked events (as described in §§IV.A) and plotted a histogram for each (see Figs. 7 and 8 for single- and multi-peaked events, respectively).

Our single-peaked burst histogram implies a unimodal

Figure 6. Distributions of δ_{90} and δ_{50} top and bottom panels, respectively, plotting frequency

distribution of T_r/T_{90} as expected. The distribution is shifted to the left which shows that most rise times are less than half of the T_{90} duration for the same burst. In fact, the highest concentration of all T_r/T_{90} ratios for single-peaked events fell between 0 and 0.1 (Fig. 7) showing that most rise times are less than 10% of the T_{90} duration.

In contrast, our multi-peaked burst histogram shows a bimodal distribution. For the multi-peaked events where the first peak was the maximum the T_r/T_{90} ratios are clustered around 0, similar to the single-peaked events. The multi-peaked events in which a later peak is brightest are responsible for the second maximum around 0.7 (Fig. 8).
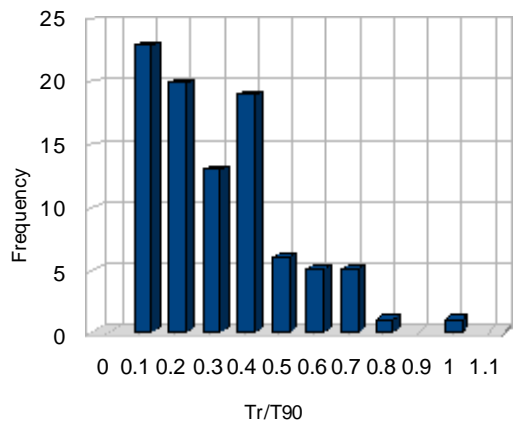

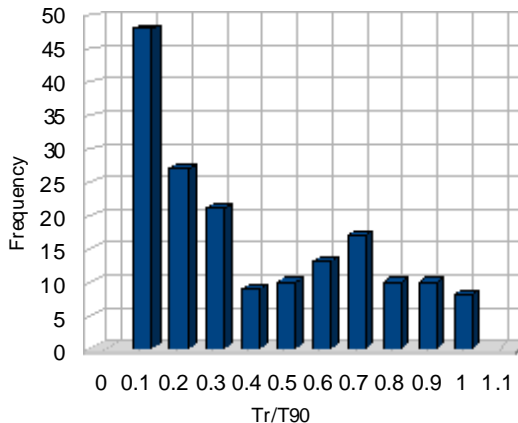Figure 8. Distribution of rise time over T_{90} for single-peaked events

Figure 8. Distribution of rise time

F. Comparative table

	SGR J1550-5418		SGR 1900+14	SGR 1806-20
	Range	Gaussian fit peak	Gaussian fit peak	Gaussian fit peak
T_{90}	23 - 1,766 ms	143.68 ms	92.4 ms	161.8 ms
T_{50}	8 - 1,192 ms	44.52 ms	–	–
τ_{90}	15 - 964 ms	80.98 ms	49.6 ms	82.3 ms
τ_{50}	6 - 338 ms	24.44 ms	–	–
δ_{90}	0.068 - 0.979	0.621	0.45	0.46
δ_{50}	0.049 - 0.968	0.585	–	–

Table 1. Comparison of SGR J1550-5418's temporal parameters with those of two other SGRs

V. Discussion

We found that the temporal parameters we measured for SGR J1550-5418, specifically T90, T50, τ90, and τ50, exhibit a single peak distribution, and are well fit by a log-normal function. These results agree with those found by Göğüş et al. (2001) for the T90 and τ90 distributions for both SGRs 1900+14 and 1806-20. Similarly, our results confirm a single-peaked distribution of the duty cycle 90 and 50 derived measurements. A log-normal function was found to fit their distribution well.

The rise time distribution measured for single-peaked bursts roughly matches the profiles of single-peaked burst rise time distributions in the SGRs analyzed by Göğüş et al. (2001), however our multi-peaked burst rise time distribution differs from the ones calculated in that study dramatically. The bimodal distribution present in our data was not found to exist in the distributions for the previously mentioned SGRs. This leads us to believe that the first burst in multi-peaked events from the other two sources is usually the brightest pulse. This is a distinguishing characteristic of SGR J1550-5418.

The peaks measured in our analysis as well as those measured by Göğüş et al. (2001) are a unique characteristic of an SGR and our calculations provide a valuable piece of the growing data base of SGR intensities.

The quantities we measured can be tied into the currently accepted crustquake model of magnetars as it has been conjectured that a greater signal brightness directly correlates with increased fissure size in the crust of a magnetar. T90 and T50 both measure the same parameter at different emission percentage thresholds. The range of T durations within our sample gives a qualitative cutoff estimate for potential fissure sizes (Table 1).

Rise times can be fit into this physical context as well. Tr is the time it takes for the twisted magnetic field to unleash its stored elastic potential energy in the form of a crust quake. After the peak brightness, the fissure continues rotating, moving to the far side of the magnetar, effectively hiding it from our instruments' field of view.

VI. References

Göğüş, Ersin et al., "Temporal and Spectral Characteristics of Short Bursts from the Soft Gamma Repeaters 1806-20 and 1900+14," *The Astrophysical* Journal. Vol. 558 No. 1, Sept. 1, 2001

Meegan, Charles et. al., "The Fermi Gamma-Ray Burst Monitor," *The Astrophysical* Journal. Vol. 702 No. 1, Sept.1, 2009

Steinle, Dr. Helmut, "Instrument", GBM Project Max-Planck-Institut für extraterrestrische Physik webpage, http://www.mpe.mpg.de/gamma/instruments/glast/GBM/www/instrument.html, [cited 6 August 2010].

Woods, Peter M., "Observations of the Bursting Pulsar and Magnetars," University of Alabama at Huntsville, Huntsville. 1999

---

†   Student Intern and researcher, NSSTC VP-62, NASA Marshall Space Flight Center